Solution structures of the cytoplasmic tail complex from platelet integrin αIIb- and β3-subunits

Aalim M. Weljie, Peter M. Hwang*, and Hans J. Vogel†

Department of Biological Sciences, University of Calgary, 2500 University Drive NW, Calgary, AB, Canada T2N 1N4

Edited by Richard O. Hynes, Massachusetts Institute of Technology, Cambridge, MA, and approved February 21, 2002 (received for review October 1, 2001)

Integrin adhesion receptors constitute a cell-signaling system whereby interactions in the small cytoplasmic domains of the heterodimeric α- and β-subunits provoke major functional alterations in the large extracellular domains. With two-dimensional NMR spectroscopy, we examined two synthetic peptides [αIIb(987MWKVGFFKRNR) and β3(716KLLITIHDRKEFAKFEEERARAKWD)] encompassing the membrane-proximal regions of the cytoplasmic domain motifs from the platelet integrin complex αIIbβ3. These membrane-proximal regions contain two conserved motifs, represented by 989KVGFFKR in the αIIb-subunit, and 716KLLITIHDR in the β3-subunit. The dimer interaction consists of two adjacent helices with residues V990 and F993 of the αIIb-subunit heavily implicated in the dimer interfacial region, as is I719 of β3. These residues are situated within the conserved motifs of their respective proteins. Further structural analysis of this unique peptide heterodimer suggests that two distinct conformers are present. The major structural difference between the two conformers is a bend in the β3-peptide between D723 and A728, whereas the helical character in the other regions remains intact. Earlier mutational analysis has shown that a salt bridge between the side chains of αIIb(R955) and β3(D723) is formed. When this ion pair was modeled into both conformers, increased nuclear Overhauser effect violations suggested that the more bent structure was less able to accommodate this interaction. These results provide a molecular level rationalization for previously reported biochemical studies, as well as a basis for an atomic level understanding of the intermolecular interactions that regulate integrin activity.

Integrins constitute a family of membrane-spanning proteins critical to maintaining tissue integrity in multicellular systems (1, 2). They have also been implicated in numerous cell-signaling processes, playing a key role in such diverse processes as hemostasis, inflammation, and wound healing (3, 4). Blood platelets possess a highly abundant system of integrin-mediated activation, and as such, platelet integrins have been well characterized at the biochemical level. Two hetero-protein domains are required for integrin function, and the αIIbβ3 heterodimer is unique to platelets. Resting αIIbβ3 has a low affinity for fibrinogen. However, after activation by an agonist, the αIIbβ3 complex switches to a high-affinity state, which causes platelets to aggregate into a hemostatic plug (5).

Integrins possess large extracellular domains with relatively small C-terminal cytoplasmic tails (typically ≈20–70 aa). Recent publication of a crystal structure for the extracellular portion of αVβ3-integrin has greatly enhanced our understanding of this region (6). A single membrane-spanning region connects the intra- and extracellular regions. The cytoplasmic tails form a crucial part of the activation mechanism as demonstrated by previous mutation studies (7–10). These studies suggest that key to integrin signaling are the highly conserved KπGFFKR and KLLvXiHDR motifs of the α- and β-cytoplasmic domains, respectively, where "X" is an unconserved residue, "π" is a conserved apolar residue, "i" is either I, F, or L, and "v" is either V, I, or M. These sequences are positioned immediately proximal to the membrane, constituting the membrane–cytoplasm interface (Fig. 1). It has been demonstrated that a short lipid-modified peptide encompassing the conserved αIIb sequence 989KVGFFKR can specifically induce platelet activation (11). It is unclear at this point exactly how the cytoplasmic tails relay messages from the cytoplasm to the extracellular space, a process termed "inside-out" signaling (5, 12). Signaling can also proceed from the "outside-in" (3), making the integrin system truly bidirectional.

Several studies with surface plasmon resonance (13), fluorescence resonance energy transfer and quenching, and circular dichroism (14) have found evidence for a direct interaction between the α- and β-cytoplasmic tails. Strong evidence reveals that this interaction is mediated, at least in part, by a salt bridge between αIIb(R995) and β3(D723) (Fig. 1) (10). Mutation of either residue to Ala results in a constitutively active αIIbβ3 complex; however, cross-substitution of these residues to reverse the charge returns the system to rest. Finally, a mixture of the cytoplasmic integrin tails has been shown to elicit polyclonal antibodies not observed for each tail in isolation (15).

Attempts at characterizing the membrane-proximal regions of both the αIIb and β3 domains by NMR spectroscopy and theoretical methods have met with limited success (16–20). In a recent ingenious study, the membrane-proximal portion of the αIIb domain was tethered to a micellar environment by a myristoyl group (18). The conserved GFFKR motif was α-helical, and the C-terminal end of the domain folded back on this motif. Another NMR study used a coiled-coil construct to tether the αIIb and β3 tails together, and although interaction between the two domains was not observed, it was found that the R724–A735 region of the β3-subunit had a propensity to form α-helical secondary structures (20). These results provide a major step forward in understanding the molecular level interactions crucial to integrin activation. However, no structural information currently exists about the direct interactions between the αIIb- and β3-cytoplasmic domains.

In the present study, we used a mixture of two synthetic peptides of the membrane-proximal regions of the integrin cytoplasmic tails which were truncated at R997 in αIIb and D740 in β3 (Fig. 1). With NMR spectroscopy, numerous contacts were observed between the highly conserved aliphatic residues in the N-terminal region of the β3-peptide and the aromatic residues in the conserved αIIb(991-GFFKR) region, indicating dimerization. Moreover, two distinct conformers were observed, and analysis of the NMR spectra indicated that the major area of deviation between the two conformers occurs between residues 719 and 725 of the β3-subunit. We present the solution structures

This paper was submitted directly (Track II) to the PNAS office.

Abbreviations: ARIA, ambiguous restraints in iterative assignments; NOE, nuclear Overhauser effect; NOESY, nuclear Overhauser effect spectroscopy.

Data deposition: The atomic coordinates and constraint lists have been deposited in the Protein Data Bank, www.rcsb.org (PDB ID codes 1KUP and 1KUZ).

*Present address: Department of Biochemistry, University of Toronto, Medical Sciences Building, 1 King's College Circle, Toronto, ON, Canada M5S 1A8.

†To whom reprint requests should be addressed. E-mail: vogel@ucalgary.ca.

The publication costs of this article were defrayed in part by page charge payment. This article must therefore be hereby marked "*advertisement*" in accordance with 18 U.S.C. §1734 solely to indicate this fact.

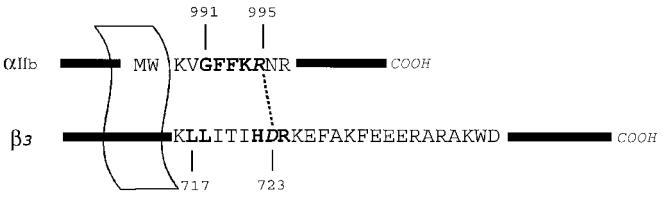

Fig. 1. Sequences used in this study of the heterodimeric αIIb- and β3-domains from platelet integrin. The C-terminal cytoplasmic tails of each domain are connected to the larger extracellular domain by singular transmembrane segments. The highlighted residues are considered highly conserved among the integrin family of proteins. The italicized residues are αIIb(R995) and β3(D723) which have been implicated in salt-bridge formation (18), depicted by the dashed line between them.

of the two conformers, which is, to our knowledge, the most detailed structural information for the dimer system to date. The two structures present a picture of integrin signaling in which the β3 (719–725) region acts as a hinge converting between helical and nonhelical conformations, possibly accounting for the switch-like behavior exhibited by platelet integrin. Because the key residues involved in the dimer interface and conformational switch are highly conserved within the integrin family, this mechanism may be more generally applicable.

Materials and Methods

Peptides. Peptides encompassing the membrane-proximal regions of platelet integrin αIIb(987 Ac-MWKVGFFKRNR-NH_2 997) and β3(716 Ac-KLLITIHDRKEFAKFEEERARAKWD-NH_2 740) were synthesized by the Peptide Synthesis Facility, Department of Chemistry, University of Waterloo, Waterloo, Canada, headed by G. Lajoie. These sequences were selected to include a single Trp residue for quantitation, and truncated to reduce overlap in the ^{1}H NMR spectra. Purity was judged to be >95% from high-pressure liquid chromatography and mass spectrometry. Quantitation of the peptides was achieved by UV spectroscopy, with an extinction coefficient of 5,500 M^{-1} cm^{-1} at 280 nm for each peptide, corresponding to the single Trp residue.

NMR Spectroscopy. An NMR sample in a 90/10% H_2O/D_2O mixture was prepared by mixing the αIIb- and β3-peptides at 2 mM in a 1:1 ratio, pH 5.2 (unbuffered) in 450 μl final volume. Solvent exchange to a 100% D_2O solution was accomplished by lyophilizing the H_2O sample to apparent dryness and then redissolving the sample in 450 μl D_2O. The pH was adjusted to 5.2, if necessary, without correction for any isotope effects. This pH was chosen to minimize the exchange rates for the amide protons (21), as is standard in the NMR analysis of small peptides and similar to the pH in previous integrin peptide structure determination (18). The addition of salt caused visible precipitation, and hence, low ionic strength conditions were used.

Total correlation spectroscopy (TOCSY) (22) and nuclear Overhauser effect spectroscopy (NOESY) (23) NMR spectra were acquired on a Bruker DRX-500 instrument by using WATERGATE (24) for water suppression at 25°C. These spectra were acquired with an initial size of 2k × 1k real and imaginary points. These spectra were zero-filled to a final size of 4k × 2k by using NMRpipe (25) and analyzed by using NMRVIEW v. 4.1.3 (26). Because of extensive overlap in the spectra, the same NMR experiments were performed on a Varian Unity Inova 800 MHz instrument spectra, and the spectra were processed to the same final size. The proton chemical shift assignment was conducted by the methods initially described by Wüthrich (21). Final spectral assignments and calibration for structure calculations were based on the 800-MHz spectra. All spectra were referenced with respect to a ^{1}H chemical shift of 0 ppm for the most upfield resonance of 5,5-dimethylsilapentanesulfonate (27).

Structure Calculations. The CNS program (version 1.0) was used for initial structure calculations, with the default values for force constants (28). Distance restraints used in structure calculations were based on the observed intensities from the NOESY spectra. Initially, calibration was achieved on the basis of strong, medium, and weak characterization, corresponding to upper bounds of 2.8, 3.4, and 5.0 Å and a lower bound of 1.8 Å. Pseudoatom corrections were applied to nonstereospecifically assigned protons as described elsewhere (29). In addition, dihedral angle restraints of −35° to −175° were used for nonglycine residues based on accepted geometry. The simulated annealing protocol was initiated from a fully extended conformation for both peptide chains.

Once structures showing convergence were achieved in CNS with no nuclear Overhauser effect (NOE) violations >0.2 Å and no dihedral violations >5°, the restraint lists were separated into two to reflect two apparent isoforms in the data. The two structures were further refined independently by using the ambiguous restraints in iterative assignments (ARIA) extension to CNS (30), with the addition of ambiguous NOE data. The default parameters were used for ARIA with the exception that the 'qmove' flag was set to on. This flag forces initially violated restraints to be reset to very weak restraints and reassessed for validity within the calibration. In the final two iterations, 100 structures were calculated, and the lowest-energy 20 were selected for the respective structure ensembles.

Once unique structures were generated representing the information from the two isoforms, a salt bridge was incorporated by imposing a 3.0-Å upper bound restraint between αIIb(R995) and β3(D723). This restraint was chosen based on generally accepted values because such salt bridges are not usually observed by means of NMR structure determination. The two structures which included the salt bridge were evaluated for likelihood of salt-bridge formation based on the overall energies and number of NOE violations as compared with the non-salt-bridged structural families. All final ensembles were evaluated by using AQUA 3.2 and PROCHECK 3.5 (31).

Results

The two peptides chosen for this study, αIIb (987–997) and β3 (717–740), represent the membrane-proximal regions of both proteins (Fig. 1). Because the peptides represent portions of larger proteins, N-terminal acetyl and C-terminal NH_2 groups were added to eliminate the terminal charges. Both peptides are void of membrane-distal motifs, which are thought to play a role in integrin regulation: αIIb(R997–D1003) (15) and β3(N744–Y747) (32). Both peptides showed little significant secondary structure in aqueous solution alone, as reported (14, 17, 20). However, under the conditions used in this study, a mixture of the two peptides demonstrated numerous clear helical $dNN_{(i,i+1)}$, $d\alpha N_{(i,i+3)}$, and $d\alpha\beta_{(i,i+3)}$ NOEs for αIIb(K989–N996), clearly indicating that this chain is an α-helix (Fig. 2). Helical structure has been reported for this portion of the αIIb sequence in 45% trifluoroethanol (17), when attached to micelles by way of lipidation (18), and when attached to a helical construct with the absence of any linker (20). In the current construct, the formation of secondary structure is favored by intermolecular contacts, as evidenced by unambiguous interchain NOEs present from the side chains of W988, V990, F992, and F993 of the αIIb peptide to I719, T720, and I721 of the β3-chain.

Conformational Exchange of the β3-Peptide. The total correlation spectroscopy and NOESY spectra from 800 MHz clearly indicated that two major conformers were present in the sample

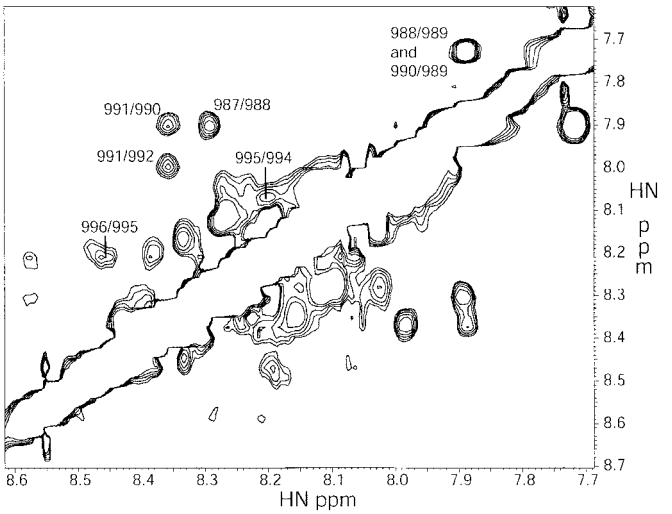

Fig. 2. Homonuclear ^{1}H NOESY spectrum at 500 MHz of the amide-amide region. This experiment provides through-space correlation of protons within 5–6 Å. The NOEs labeled are indicative of strong helical structure for the αIIb peptide. Note that potential correlations for αIIb (989/990, 992/993, and 993/994) are obscured by the diagonal. The remaining peaks show helical propensity of the β3-peptide, although ambiguity and conformational exchange make this analysis more difficult. Note the difference in intensity for the αIIb peaks (with labels), and the remaining β3 peaks.

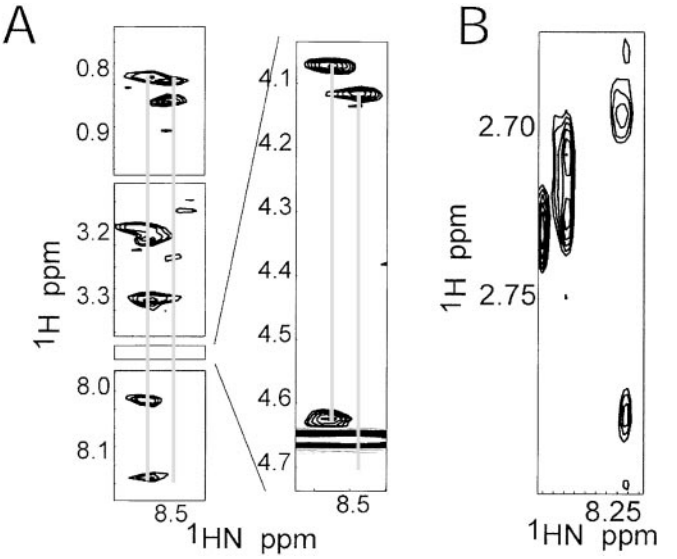

Fig. 3. NOESY spectrum at 800 MHz in which conformational exchange is demonstrated by amide chemical shift duplication for residues (*A*) β3(H722) and (*B*) β3(D723). Both of these cases demonstrate the slow exchange which results in the conclusion that two distinct conformers exist in solution for the β3-peptide. In *A*, the conformation of the His residue on the downfield (*Left*) side participates in some type of helical secondary structure as evidenced by the dNN NOEs, which corresponds to structure αIIbβ3-2 in the current study. Also notice that although both His conformations show strong NOEs with the Hα from β3(I721) (*Insert*), only the downfield conformation has a strong intraresidue HN-Hα NOE. In *B*, the β-proton region is shown, with the downfield conformation suggesting two protons with near-degenerate chemical shifts, whereas the protons in the upfield conformation exhibit distinct chemical shifts.

(Fig. 3). The presence of these conformers is unusual given that the system in question consists of two relatively short peptide chains (11 and 25 aa) with no Pro or Cys residues, and any conformational exchange would be expected to be rapid. A near-complete assignment of both conformers was obtained from the spectra at 800 MHz. The most evident conformational difference was later localized to a specific region of the β3-peptide backbone. This region showing the greatest chemical shift differences, β3(719–725), encompasses β3(D723), which is implicated in a charged interaction with αIIb(R995) (10). Analysis of the β3 NOEs was much less trivial than that of the αIIb because of these conformation differences and weaker NOE peaks. Nonetheless, helical NOEs were clearly observed for the β3-peptide (Fig. 2), which is consistent with modeled data (16) and NMR analysis (20). The latter study demonstrated that the region R724–A735 had helical propensity, and that the membrane-proximal region also formed an α-helix when stabilized by helix propagation. In our study, interchain contacts are apparent in the β3-membrane-proximal region L717–D723, presumably reducing flexibility and increasing the manifestation of the intrinsic helical character in this region.

NMR Structures. As a result of the structural ambiguity due to conformational exchange as discussed above, we proceeded with the structural characterization of two conformers from the αIIbβ3-peptide complex independently. Once reasonable convergence was achieved with the major NOEs common to both models, the divergent backbone NOEs were easily distinguished in both the H_2O and D_2O spectra, but side-chain chemical shift differences were much less obvious because of overlap and weak intensities. As a result, all ambiguous side-chain NOEs were included resulting in a relatively large number of NOEs (Table 1), and violated NOEs were excluded by ARIA in the final calculations. In addition, some intrapeptide NOE intensities for the αIIb-peptide were very intense for certain aliphatic residues (e.g., M987 and V990) and were also violated in the ARIA calibration routine. The two models based on the dual conformations are referred to as αIIbβ3-1 and αIIbβ3-2, and Table 1 presents summary statistics for both. Conformational differences and violated NOE patterns suggest a view of a dynamic system, and the structures calculated are most likely average representatives of an ensemble of states. Inclusion of NOEs from these mixed states may lead to an "overconvergence" of the data into an unrealistically tight set of structures as demonstrated by the surprisingly small rms deviation values (Table 1). Despite this caveat, it is still clear that structures provide a picture of heterodimeric interaction that is consistent with the NOE data.

Fig. 3 shows that in both conformers, the αIIb- and β3-chains demonstrate significant helical character. Significant hydrophobic interactions occur between αIIb(V990, F993) and β3(L717–I21), which are critical residues of the dimer interface (Fig. 4). The reported structure of a membrane-anchored lipidated αIIb cytoplasmic tail also demonstrated that V990 and F993 form a hydrophobic interaction surface, with F992 on the opposite side of the helix (18). It is not surprising that the F993 region is implicated in dimerization considering that the GFFKR motif is highly conserved in the integrin family. Unambiguous NOEs were observed between the αIIb(F992) side chain and β3(I719), but these were weak, and F992 does not seem to be as central to the dimer interface as V990 and F993.

Although the αIIb-peptide maintains a helical conformation with one major helical turn in both structures, the divergence is significant in the backbone conformation of the β3-peptide, as expected from the NOE data (Fig. 2). In both cases, helical propensity is clearly displayed between residues K716–I721 and K729–W739. Particularly interesting is the contrast between the two structures in the region D723 to A728. In the αIIbβ3-2 conformer, this region is somewhat helical, so that the entire β3-peptide adopts an elongated and primarily helical structure. On the other hand, in the αIIbβ3-1 model, the D723–A728

Table 1. Final structural data for αIIbβ3 complexes, with and without salt bridge

Distance restraints (NOE)	αIIbβ3-1	αIIbβ3-2
Unambiguous	649	627
Sequential	182	171
Medium range	252	251
Interchain	25	22
Ambiguous	337	366
Ramachandran plot (%)		
Most favored regions	47.1	67.3
Additionally allowed regions	46.6	32.7
Generously allowed regions	2.9	0.0
Disallowed regions	0.0	0.0
Ideal geometry rms deviation (A^2)		
Bonds	0.004 ± 0.000	0.004 ± 0.000
Angles	0.543 ± 0.008	0.586 ± 0.029
Impropers	0.412 ± 0.013	0.367 ± 0.027
ARIA final energy of ensemble	281.82 ± 6.15	233.25 ± 14.24
rms deviation to average structure (well-defined regions) (A^2)		
Backbone	0.600	0.753
Heavy atoms	1.198	1.486
After including salt-bridge restraint		
ARIA final energy	248.18 ± 5.02	217.04 ± 9.26
Change in ARIA consistent violations	+11	−7
Ramachandran plot (%)		
Most favored regions	47.1	65.6
Additionally allowed regions	52.1	34.4
Generously allowed regions	0.8	0.0
Disallowed regions	0.0	0.0
rms deviation to average structure (well-defined regions) (A^2)		
Backbone	1.004	0.885
Heavy atoms	1.507	1.505

region is clearly not helical and bends back toward the membrane-proximal region, causing the β3-peptide to close in an "L"-like form as shown in Fig. 5. The D723–A728 sequence can be seen as a hinge region in the complex, allowing movement of the two helical areas of β3 with respect to each other.

One consequence of the variability in the β3-hinge region is the rearrangement of the αIIb-peptide with respect to the β3-membrane-proximal region (Fig. 6). In the structures we have calculated, the C-terminal tail of the β3-peptide folds back toward the αIIb-peptide in the αIIbβ3-1 conformer causing this displacement (Fig. 6*A*). Fig. 6*B* shows that this movement causes the αIIb peptide to be slightly displaced, although it maintains the same structure (Fig. 6*B*). Not represented in either structure is NOE evidence suggesting that the closure of the β3-peptide may be even greater than what is represented in conformer αIIbβ3-1. There were two unambiguous intrachain long-range NOEs unsatisfied in either structure observed between the side chain of β3(W739) and β3(I719), which would necessitate a more extreme turn than exists in αIIbβ3-1. These long-range β3-intrapeptide NOEs suggest a complete displacement of αIIb, or at least a more serious rearrangement of the dimer complex, although it was not possible to establish how the αIIb-peptide would have to be displaced by the results of the current study. The fact that these NOEs were unsatisfied further underscores the fact that the system is dynamic, and many of the observed dimer contacts may be transitory. In other words, the αIIbβ3-1 conformation may be the average of an extended and a fully closed state. Nevertheless, each conformer model is likely representative of an ensemble of states.

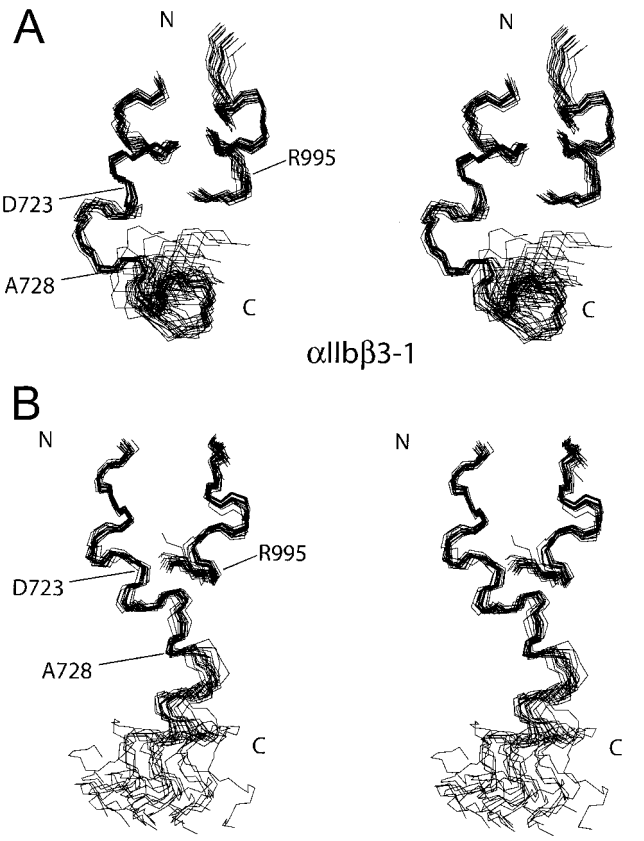

Fig. 4. Stereo images of the family of 20 lowest-energy structures calculated for the αIIbβ3-peptide complex studied in αIIbβ3-1 (*A*) and αIIbβ3-2 (*B*) . The shorter peptide corresponds to αIIb, and the longer slightly less ordered one, β3. Note that in both ensembles the region near the dimer interface is well ordered, as residues αIIb (988–996) and β3 (718–736) are fitted to the average structure. When the C-terminal portion of the β3-peptide is fit alone, i.e., β3 (729–740), excellent convergence also occurs (i.e., residues 728–739). This figure was generated with MOLMOL (40).

Modeling of the αIIb(R995)–β3(D723) Salt Bridge. Because charge-swapping mutational analysis suggests that interactions between the highly conserved αIIb(R995) and β3(D723) residues are critical to integrin function (10), we examined the effect of this ionic interaction on our models. NOE evidence was not apparent in our spectra to support such an interaction, although this is expected given the 5–6 Å upper limit in observable proton NOEs. As a result, we incorporated a restraint for the ionic interaction in the proposed salt bridge into both conformers. In both cases the side chain of αIIb(R995) moved from a solvent-exposed state to the bridged state, with a minor readjustment of the C-terminal portion of the αIIb peptide (not shown). Table 1 presents energy and Ramachandran statistics for structures calculated with the same input data sets as αIIbβ3-1 and αIIbβ3-2, respectively. In αIIbβ3-1, the number of restraints excluded by the ARIA calibration routine increased. In contrast, the number of excluded restraints for αIIbβ3-2 actually decreased, indicating that the salt bridge most likely forms from the αIIbβ3-2 conformer (Fig. 5*C*). Addition of the salt bridge allowed an NOE between αIIb(W988) and β3(I719) to be satisfied, previously the only unsatisfied interchain restraint. The remaining unsatisfied restraints were either intrachain αIIb restraints (totaling 12) or ambiguous (totaling 2). The fact that these are primarily from the αIIb peptide is understandable, given that peak intensities for the β3-peptide are dispersed between at least two conformations. This causes intrachain αIIb

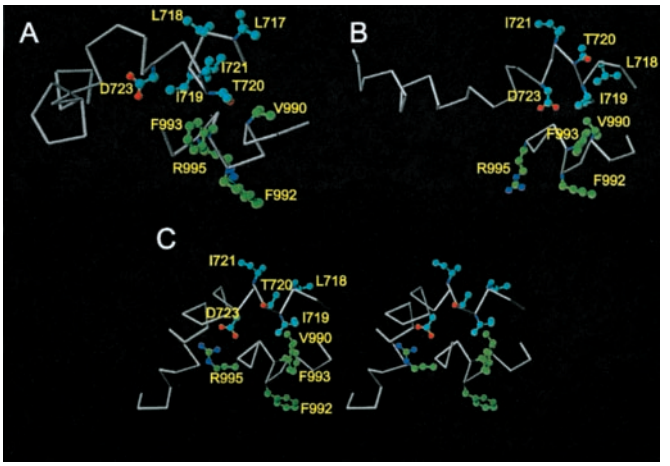

Fig. 5. Cα trace of the average calculated structure based on the ensemble of 20 lowest-energy structures for the αIIbβ3-peptide complex in this study: (*A*) αIIbβ3-1; (*B*) αIIbβ3-2; and (*C*) αIIbβ3-2 with salt-bridge constraint (stereo image). In all structures, the αIIb-peptide forms a single-turn helix, whereas the β3-peptide has significant helical character. Also common to the structures are significant interactions between the side-chain moieties of αIIb(V990, F993) with the aliphatic β3(I719) residue. A significant difference exists in the β3 chain; however, as in αIIbβ3-1 a bend between residues D723 and A728 forces the C-terminal tail closer to the N terminus, creating an ''L''-like shape. This may be a determining factor in the movement of the αIIb-peptide, as shown in Fig. 6.

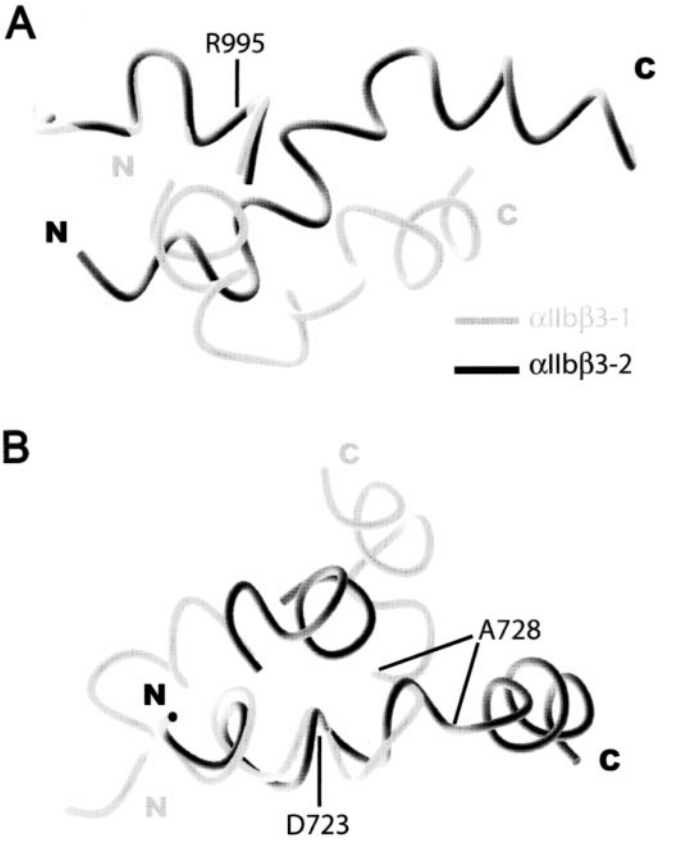

Fig. 6. Superposition of the N-terminal backbone region for the two conformers, with coloration as indicated. (*A*) Residues αIIb (988–996) and (*B*) residues β3 (718–728) were used for fitting. The orientation of the complex in *A* is the same as in Fig. 4 with a 90° rotation, and *B* shows the displacement of the αIIb-peptide. In the αIIbβ3-1 model, the C-terminal tail from β3 wraps back on the rest of the complex, presumably forcing the αIIb peptide to twist slightly, although it maintains essentially the same structure. This figure was generated with MOLMOL (40).

NOEs to be disproportionately large. It is worth noting, however, that all interchain and β3-NOEs are satisfied between the three structures: αIIbβ3-1, αIIbβ3-2, and αIIbβ3-2 with a salt-bridge constraint, with the exception of the long-range β3 restraint mentioned above (W739–I719).

Discussion

One of the key features of the integrin cell-signaling system is the on-off mechanism of activation. The structures presented here strongly support the conclusion that this on-off mechanism is mediated by direct interaction between the conserved residues in the membrane-proximal portion of the cytoplasmic tails of the αIIb and β3 domains. The current study shows that the membrane-proximal region of β3 forms an α-helix, much like that of αIIb (17, 18), suggesting that these sequences form rigid continuations of the transmembrane helices. Glycosylation studies indeed suggest that the C-terminal end of the transmembrane segment of the integrin subunits extend into what is traditionally viewed as the membrane-proximal region of the cytoplasmic domains (33). Thus, the suggestion that the rearrangement necessary to find stable helix-interacting states (or a complete separation of the helices) can translate through the membrane-spanning regions to cause a global shift in the extracellular domains is quite reasonable.

The key residues in the αIIbβ3-dimer interface are V990 and F993 from αIIb and I719 from β3, indicating a predominantly hydrophobic interaction. αIIb(F993) is a key residue in forming the hydrophobic patch in the dimer, and enough contacts exists to provide a well-defined picture of the dimer interface. In a previously solved structure of the αIIb-cytoplasmic domain, the 11 residues at the C terminus were found to fold back and interact with the helical N-terminal portion of the peptide (18), and several long-range NOEs to F993 were observed. For the αIIbβ3 dimer to form, the C-terminal portion of the αIIb tail may need to be displaced. Stabilization of the closed conformation in full-length αIIb-peptide may partially explain why other groups have not been able to observe dimerization in their NMR experiments. In addition, all of the interchain NOEs evident from our work involved methyl and aromatic side-chain protons, which would not have been considered in the ^{15}N-edited spectra considered by other recent NMR analyses (19, 20).

The translation of the αIIb-peptide with respect to the β3-peptide between the two conformers of this study suggests that the hydrophobic patch is large or flexible enough to accommodate such a motion. It is not surprising then that the samples displayed marked salt-dependent aggregation not seen under similar conditions with either peptide in isolation, and low ionic strength conditions were required for the complex. Presumably, *in vivo* the presence of the remainder of the integrin subunits, membrane proximity, and/or other protein interactions mitigate these aggregation effects. Further work needs to be done to characterize the residues involved in this aggregation to establish the physiological consequences of this result.

The structural similarities between the αIIb- and β3-cytoplasmic tails extend beyond the helical membrane proximal regions. Both are immediately followed by a flexible hinge: ^{998}PPLEED in αIIb and ^{723}DRKEFA in β3. (The presence of multiple charged residues in the β3-hinge suggests that its conformation may be very sensitive to ionic interactions.) This flexibility creates a conformational switch, allowing C-terminal regulatory sequences to be brought into close proximity of the membrane proximal region. For a double mutant peptide of αIIb(P998A, P999A) which did not fold back on itself, the αIIbβ3 system was fixed in a constitutively active state (18).

Both αIIb- and β3-cytoplasmic domains interact with cytosolic proteins which seem to bind sequences on both sides of the flexible hinge region. This seems to be true of calcium- and integrin-binding protein, a calmodulin-like protein (18, 34). β_3-Endonexin requires both the membrane proximal sequence and ^{756}NITY for binding (35), whereas talin seems to require both the membrane-proximal sequence (36) and ^{744}NPLY (20) for binding. The binding pattern of these proteins suggests that the NITY and NPLY sequences are able to fold into close proximity of the membrane-proximal region.

The β3-hinge region plays a key role in determining the nature of the membrane-proximal αIIbβ3 interface, which in turn likely determines the activation state of the αIIbβ3 system. In the current study, the experimental system seems to be teetering between two major states, although the exact physiological relevance of the two states is unclear. We propose that the αIIbβ3-2 conformer, which is more amenable to the intermolecular αIIb(R995)–β3(D723) salt bridge, corresponds to the resting low-affinity state. We suggest that the αIIbβ3-1 conformer (or a more bent form in which the αIIb-subunit is further displaced) is representative of the activated high-affinity state. This suggestion is consistent with two recent studies which indicate that the inactive form is based on a coiled-coil interaction (37), and that spatial separation of the two membrane-proximal regions leads to activation (38). Such activation might correspond to either a ''piston'' or ''twist'' model of inside-out signaling as outlined by Ginsberg and coworkers (39). Clearly, more detailed structural analysis involving mutants would be helpful. As well, it is still far from clear what roles the membrane-distal regions of both cytoplasmic tails play in this balancing act, and how they are affected by the plethora of cytoplasmic integrin-binding proteins identified thus far.

We thank Dr. Stéphane M. Gagné for acquisition of spectra at 800 MHz. We thank the Canadian National High Field NMR Centre (NANUC) for their assistance and use of the facilities. Operation of NANUC is funded by the Canadian Institutes of Health Research, the Natural Science and Engineering Research Council (NSERC) of Canada, and the University of Alberta. A.M.W. is a recipient of graduate scholarships from NSERC and the Alberta Heritage Foundation for Medical Research (AHFMR). H.J.V. is an AHFMR Senior Scientist. This work was supported by operating grants from the Canadian Institutes of Health Research and the Alberta Heart and Stroke Foundation.

1. Giancotti, F. G. & Ruoslahti, E. (1999) *Science* **285,** 1028–1032.
2. Hynes, R. O. & Zhao, Q. (2000) *J. Cell Biol.* **150,** F89–F96.
3. Hynes, R. O. (1992) *Cell* **69,** 11–25.
4. Clark, E. A. & Brugge, J. S. (1995) *Science* **268,** 233–239.
5. Shattil, S. J. (1999) *Thromb. Haemostasis* **82,** 318–325.
6. Xiong, J. P., Stehle, T., Diefenbach, B., Zhang, R., Dunker, R., Scott, D. L., Joachimiak, A., Goodman, S. L. & Arnaout, M. A. (2001) *Science* **294,** 339–345.
7. O'Toole, T. E., Mandelman, D., Forsyth, J., Shattil, S. J., Plow, E. F. & Ginsberg, M. H. (1991) *Science* **254,** 845–847.
8. O'Toole, T. E., Katagiri, Y., Faull, R. J., Peter, K., Tamura, R., Quaranta, V., Loftus, J. C., Shattil, S. J. & Ginsberg, M. H. (1994) *J. Cell Biol.* **124,** 1047–1059.
9. Briesewitz, R., Kern, A. & Marcantonio, E. E. (1995) *Mol. Biol. Cell* **6,** 997–1010.
10. Hughes, P. E., Diaz-Gonzalez, F., Leong, L., Wu, C., McDonald, J. A., Shattil, S. J. & Ginsberg, M. H. (1996) *J. Biol. Chem.* **271,** 6571–6574.
11. Stephens, G., O'Luanaigh, N., Reilly, D., Harriott, P., Walker, B., Fitzgerald, D. & Moran, N. (1998) *J. Biol. Chem.* **273,** 20317–20322.
12. Hughes, P. E. & *Pfaff*, M. (1998) *Trends Cell Biol.* **8,** 359–364.
13. Vallar, L., Melchior, C., Plancon, S., Drobecq, H., Lippens, G., Regnault, V. & Kieffer, N. (1999) *J. Biol. Chem.* **274,** 17257–17266.
14. Haas, T. A. & Plow, E. F. (1996) *J. Biol. Chem.* **271,** 6017–6026.
15. Ginsberg, M. H., Yaspan, B., Forsyth, J., Ulmer, T. S., Campbell, I. D. & Slepak, M. (2001) *J. Biol. Chem.* **276,** 22514–22521.
16. Haas, T. A. & Plow, E. F. (1997) *Protein Eng.* **10,** 1395–1405.
17. Hwang, P. M. & Vogel, H. J. (2000) *J. Mol. Recognit.* **13,** 83–92.
18. Vinogradova, O., Haas, T., Plow, E. F. & Qin, J. (2000) *Proc. Natl. Acad. Sci. USA* **97,** 1450–1455.
19. Li, R., Babu, C. R., Lear, J. D., Wand, A. J., Bennett, J. S. & DeGrado, W. F. (2001) *Proc. Natl. Acad. Sci. USA* **98,** 12462–12467.
20. Ulmer, T. S., Yaspan, B., Ginsberg, M. H. & Campbell, I. D. (2001) *Biochemistry* **40,** 7498–7508.
21. Wuthrich, K. (1986) *NMR of Proteins and Nucleic Acids* (Wiley, New York).
22. Braunschweiller, L. & Ernst, R. R. (1983) *J. Magn. Reson.* **53,** 521–528.
23. Jeener, J., Meier, B. H., Bachmann, P. & Ernst, R. R. (1979) *J. Chem. Phys.* **71,** 4546–4553.
24. Piotto, M., Saudek, V. & Sklenar, V. (1992) *J. Biomol. NMR* **2,** 661–665.
25. Delaglio, F., Grzesiek, S., Vuister, G. W., Zhu, G., Pfeifer, J. & Bax, A. (1995) *J. Biomol. NMR* **6,** 277–293.
26. Johnson, B. A. & Blevins, R. A. (1994) *J. Biomol. NMR* **4,** 603–614.
27. Markley, J. L., Bax, A., Arata, Y., Hilbers, C. W., Kaptein, R., Sykes, B. D., Wright, P. E. & Wuthrich, K. (1998) *J. Biomol. NMR* **12,** 1–23.
28. Brunger, A. T., Adams, P. D., Clore, G. M., DeLano, W. L., Gros, P., Grosse-Kunstleve, R. W., Jiang, J. S., Kuszewski, J., Nilges, M., Pannu, N. S., *et al.* (1998) *Acta Crystallogr. D. Biol. Crystallogr.* **54,** Part 5, 905–921.
29. Wuthrich, K., Billeter, M. & Braun, W. (1983) *J. Mol. Biol.* **169,** 949–961.
30. Nilges, M. & O'Donoghue, S. I. (1998) *Prog. NMR Spectroscopy* **32,** 107–139.
31. Laskowski, R. A., Rullman, J. A. C., MacArthur, M. W., Kaptein, R. & Thornton, J. M. (1996) *J. Biomol. NMR* **8,** 477–486.
32. O'Toole, T. E., Ylanne, J. & Culley, B. M. (1995) *J. Biol. Chem.* **270,** 8553–8558.
33. Armulik, A., Nilsson, I., von Heijne, G. & Johansson, S. (1999) *J. Biol. Chem.* **274,** 37030–37034.
34. Naik, U. P., Patel, P. M. & Parise, L. V. (1997) *J. Biol. Chem.* **272,** 4651–4654.
35. Eigenthaler, M., Hofferer, L., Shattil, S. J. & Ginsberg, M. H. (1997) *J. Biol. Chem.* **272,** 7693–7698.
36. Patil, S., Jedsadayanmata, A., Wencel-Drake, J. D., Wang, W., Knezevic, I. & Lam, S. C. (1999) *J. Biol. Chem.* **274,** 28575–28583.
37. Lu, C., Takagi, J. & Springer, T. A. (2001) *J. Biol. Chem.* **276,** 14642–14648.
38. Takagi, J., Erickson, H. P. & Springer, T. A. (2001) *Nat. Struct. Biol.* **8,** 412–416.
39. Williams, M. J., Hughes, P. E., O'Toole, T. E. & Ginsberg, M. H. (1994) *Trends Cell Biol.* **4,** 109–112.
40. Koradi, R., Billeter, M. & Wuthrich, K. (1996) *J. Mol. Graph.* **14,** 51–32.